Driven particle in an infinite square well: Representation and breakdown of the invariant tori in a multiple-resonance case

M. Z. Fuka, J. K. McIver, and W. Becker
Department of Physics and Astronomy, University of New Mexico, Albuquerque, New Mexico 87131

M. Orszag and R. Ramírez
Facultad de Física, Universidad Católica de Chile, Casilla 6177, Santiago 22, Chile
(Received 21 October 1993; revised manuscript received 27 June 1994)

This paper describes the representation and breakdown of the invariant Kol'mogorov-Arnol'd-Moser (KAM) tori of the driven particle in an infinite square well in terms of the periodic trajectories of the system. The periodic cycles are characterized analytically and numerically and their stability as the amplitude of the driving field increases is determined numerically. A representation of the zoning number, analogous to the winding number of the standard map, is developed for the system. It is shown that a KAM surface can be approximated by high-order periodic cycles with winding numbers corresponding to continued fraction approximates of the KAM surface's irrational zoning number. The zoning numbers of the most robust KAM tori between primary resonances are related to the golden mean and approximated accordingly by periodic cycles. The critical fields at which the invariant tori break down and the accompanying transition from local to global stochasticity occurs is estimated from the breakdown fields of the cyclic approximates.

PACS number(s): 05.45.+b

I. INTRODUCTION

The motion of a particle in a one-dimensional infinite square well potential driven by an external time-dependent cosine field is a nonlinear conservative system that is conceptually and mathematically straightforward, yet maintains enough structure to be useful in modeling actual physical systems [1]. As such, the driven square well is a valuable example for theoretical study of nonlinear systems. An analysis of the transition to global chaos in the classical system is presented by Lin and Reichl [2,3]. As in other such Hamiltonian systems [3–7], the classical trajectories (or "orbits" or "cycles") of the particle in this one-dimensional system lie on toroidal surfaces with cross sections dependent on position and momentum or transformations of these coordinates and an interior angle that is a function of time.

For extremely small perturbing fields, trajectories lie on islands surrounding stable (elliptic) fixed points in phase space, are confined to narrow stochastic layers bounded by Kol'mogorov-Arnol'd-Moser (KAM) trajectories, or are themselves KAM tori. As the field amplitude increases, the infinite number of primary resonances widens, a complex structure of secondary islands emerges, and the stochastic layers broaden as bounding KAM surfaces disintegrate. When the most robust KAM surface between primary resonances breaks down, the resonance zones merge with the stochastic sea. For the infinity of principal resonances characterizing the driven square well, the effect is that of a cascade of sharply defined breakdowns between neighboring primary resonances, proceeding from higher- to lower-order resonance pairs.

Lin and Reichl use a renormalization method developed by Escande and Doveil for two-resonance Hamiltonian systems [8] to estimate the critical field at which the most stable KAM surfaces break down in the driven square well. Their predictions of critical fields compare very well to numerical experiment and are considerably more accurate than overestimates typically obtained from the Chirikov overlap criterion and its variants [4]. The focus of Lin and Reichl's study of the system is on estimating critical fields rather than describing the KAM surfaces themselves, a natural approach to defining the limit to which a physical system can be pushed before it becomes completely stochastic and all ability to predict behavior is lost. When an explicit description of the KAM surfaces is required, however, difficulties arise. As nonperiodic trajectories, KAM surfaces are characterized by irrational winding or rotation numbers and cannot be represented exactly using numerical methods. We address these difficulties by applying concepts developed by Escande for two-resonance systems to approximating the KAM surfaces in the driven square well.

Escande [9] links the original renormalization method to periodic continued fraction approximates of KAM surfaces through the "zoning number." The zoning number's role is analogous to that played by the winding number in the special case of the standard map [10], uniquely ranking trajectories in the resonance hierarchy. Escande approximates KAM tori in the general two-resonance system with a sequence of increasingly high-order periodic trajectories whose zoning numbers are the continued fraction approximations of the irrational KAM trajectory zoning numbers. The breakdown of the KAM surfaces is estimated by the transitions from stability to instability of those cycles, with successively higher-order cycles providing improved estimates. The most robust KAM

surface between primary resonances possesses a zoning number equal to the golden mean or its near equivalent. Determining the last KAM breakdown therefore becomes a matter of specifying the periodic trajectories of the system and determining their stability, a more manageable problem than that of attacking the KAM trajectories directly.

The research discussed in this paper uses these ideas to derive a detailed classical description of the periodic trajectories and KAM surfaces of the driven square well. Section II reviews the equations of motion for the system. Section III discusses the calculation of periodic trajectories, a task that requires solving $2n+1$ nonlinear equations of motion by an iterative numerical scheme. Section IV presents a first-order linear stability analysis of the periodic cycles and calculations of the critical fields at which those trajectories become unstable. Section V begins with a review of Lin and Reichl's derivation of the approximate two-resonance paradigm form of the Hamiltonian and a brief description of Escande's zoning number theory [2,9]. We derive a relationship between the Escande zoning number and the winding number in the original system and then use this relation to develop a detailed description of the most robust KAM surfaces of the system based on those of its two-resonance approximation. Finally, we estimate the fields at which these tori break down. These estimates prove to agree closely with previous results and numerical experiment. Because the KAM surfaces themselves are described, this work provides a considerably more complete picture of the KAM structure than was previously available.

The original motivation for acquiring a more complete understanding of this driven system was to increase its usefulness as a model for the process of laser damage in dielectric materials [1]. In light of work in quantum chaotic Hamiltonian systems, our description of the periodic cycles proves interesting beyond its application to modeling KAM tori. Lin and Reichl have extended the concept of resonance overlap to the quantum square well [11,12] and Gutzwiller has shown that the structure of periodic trajectories in a classical system is intimately related to the structure of the system's energy levels in the quantum regime [7]. We have been able to apply the descriptions of classical periodic and KAM trajectories presented in this paper to the problem of determining KAM equivalents in the quantum mechanical system, work that we will describe in later works [13,14].

II. EQUATIONS OF MOTION

We begin with a brief review of the classical equations of motion for the driven square well (Fig. 1). The width of the square well is $2a$, the left- and right-hand walls are located at $-a$ and $+a$, respectively, a is set to 1, and the mass of the particle is set to $\frac{1}{2}$. The equation of motion for the particle as it moves between the walls is

$$\ddot{x} = -2\varepsilon \cos \omega t. \tag{1}$$

The solution of this equation for particle position $x(t)$ and momentum $p(t)$ between wall contacts is

$$x(t) = x_I + \frac{2\varepsilon}{\omega^2}(\cos\omega t - \cos\omega t_I) + \left(\frac{2\varepsilon}{\omega}\sin\omega t_I + 2p_I\right)(t - t_I),$$
$$p(t) = p_I - \frac{\varepsilon}{\omega}(\sin\omega t - \sin\omega t_I), \tag{2}$$

where the subscript I indicates the initial time, position, and momentum.

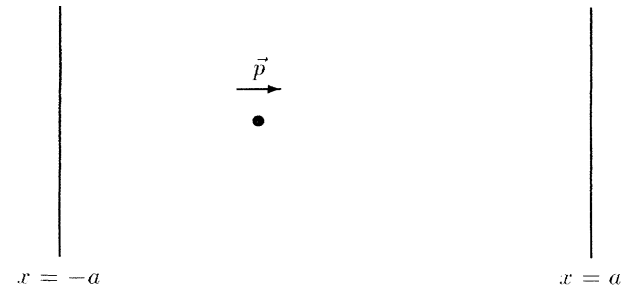

FIG. 1. Particle in an infinite square well, walls at $-a$ and a.

The calculation of a complete trajectory requires reformulation of its equations at each wall contact to account for the momentum reversal. Position, momentum, and time at the contact are used as the initial conditions for the subsequent motion. The recast equations for particle position $x_s(t)$ and momentum $p_s(t)$ at time t between the sth and $(s+1)$th contacts occurring at times t_s and t_{s+1}, respectively, are given by

$$x_s(t) = a_s + b_s t + \kappa \cos\omega t,$$
$$p_s(t) = \frac{1}{2}(b_s - \kappa\omega \sin\omega t),$$
$$t_s < t < t_{s+1},\ s = 1, 2, \ldots, \tag{3}$$

where $\kappa = (2\varepsilon)/\omega^2$ and the coefficients a_s and b_s are given by

$$a_s = x_s(t_s) - \kappa\cos\omega t_s - b_s t_s\ ,$$
$$b_s = 2p_s(t_s) + \kappa\omega\sin\omega t_s\ . \tag{4}$$

Boundary conditions at time t_s are

$$x_s(t_s) = x_{s-1}(t_s),$$
$$p_s(t_s) = -p_{s-1}(t_s), \qquad s > 1\ . \tag{5}$$

The equations of motion and boundary conditions are used to calculate particle trajectories numerically, given a set of initial conditions $[x_I(t_I), p_I(t_I)]$. Calculated particle trajectories are viewed in stroboscopic plots (Fig. 2) in which particle position and momentum are plotted at times $2\pi N$ for $N = 1, 2, \ldots$. The Poincaré section shown in Fig. 2 illustrates the complex structure of separatrices,

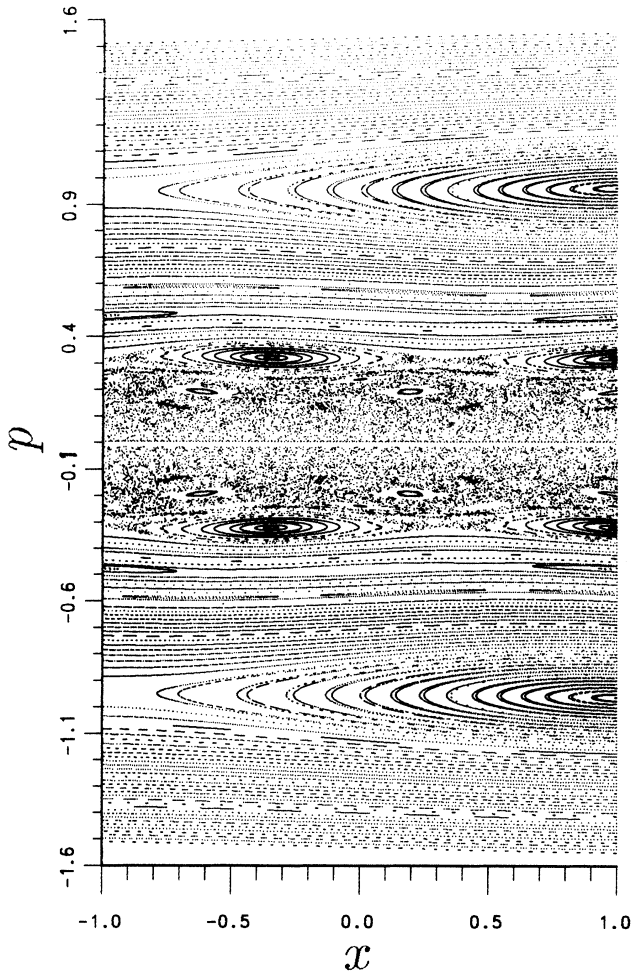

FIG. 2. Phase space strobe plot of 100 trajectories at field strength $\varepsilon = -0.04$, with momentum p plotted versus position x. The initial momentum p_I of the 100 trajectories varies from -0.01 to -1.00 in increments of 0.04. The initial position x_I is at the right-hand wall and initial time and field phase are zero. The solid lines indicate the odd-numbered primary resonance zones. All calculations presented in this paper were performed on a Sun Sparc 10 workstation.

stochastic layers, stable islands surrounding periodic trajectories, and KAM approximations. At very low particle momenta, the structure merges into a region of entirely chaotic motion. The recursive form of the equations of motion (3) makes it convenient to consider a trajectory in terms of the times at which the particle hits the well walls. Throughout this work, a trajectory is specified as a set of wall contact times and an initial position and momentum.

The focus of this paper is restricted to the most physically interesting particle trajectories, those for which the electric field perturbs rather than dominates the motion. For these trajectories, the particle alternates between walls, never hitting the same wall twice in succession. The boundary condition at the walls is

$$x_s(t_s) = (-1)^{s+1} x_1(t_1), \qquad s = 1, 2, \ldots , \tag{6}$$

where t_1 is the time of the first wall contact, that is,

$$x_1(t_1) = \pm 1. \tag{7}$$

The coefficients a_s and b_s (4) can be rewritten

$$\begin{aligned} a_s &= (-1)^s (a_I - 2sx_1) \\ &\quad -2\kappa \sum_{r=1}^{s} (-1)^{r+s} (\omega t_r \sin \omega t_r + \cos \omega t_r), \\ b_s &= (-1)^s b_I + 2\kappa\omega \sum_{r=1}^{s} (-1)^{r+s} \sin \omega t_r \ , \end{aligned} \tag{8}$$

where

$$a_I = x_I - \kappa, \quad b_I = 2p_I. \tag{9}$$

Substituting these expressions into (3) yields a recursive form of the equations of motion in terms of the initial momentum and wall contact times [$x_1 \equiv x_1(t_1)$]:

$$\begin{aligned} (-1)^{s+1} x_1 &= a_I - 2sx_1 \\ &\quad +2\kappa \sum_{r=1}^{s-1} (-1)^r [\omega(t_s - t_r) \sin \omega t_r - \cos \omega t_r] \\ &\quad +b_I t_s + (-1)^{s+1} \kappa \cos \omega t_s . \end{aligned} \tag{10}$$

The summations in this expression are eliminated by combining the equations for t_s, t_{s+1}, and t_{s+2}, resulting in a three-term recursion relation for the contact times:

$$\begin{aligned} 2\kappa\omega \sin \omega t_{s+1} &= \frac{2x_1(-1)^{s+1} - \kappa(\cos \omega t_{s+2} - \cos \omega t_{s+1})}{t_{s+2} - t_{s+1}} \\ &\quad - \frac{2x_1(-1)^{s+1} + \kappa(\cos \omega t_{s+1} - \cos \omega t_s)}{t_{s+1} - t_s} . \end{aligned} \tag{11}$$

In addition to initial conditions and contact times, each trajectory is also associated with a winding number ρ, defined as the number of spatial periods completed in one period of the driving field. The winding number is given by

$$\rho = \frac{\bar{v} T}{\lambda} \ , \tag{12}$$

where $\bar{v}$ is the mean particle velocity, T is the time required to complete a single cycle of the field, and λ is the distance traveled in one spatial period of the particle motion, i.e., twice the well width. Periodic trajectories are characterized by rational winding numbers, KAM surfaces by irrational winding numbers.

III. PERIODIC TRAJECTORIES

In a periodic motion the particle makes a total of $2n$ wall contacts in alternation in exactly N complete field

cycles (total time $2N\pi/\omega$), returning to the initial position with the initial velocity. A periodic orbit is referred to as an (n, N) cycle. The cycle has a rational winding number of form

$$\rho = \frac{n}{N} , \tag{13}$$

where n and N are integers. The class of periodic cycles with the same spatial periodicity, i.e., those associated with the same value of n, are referred to as n cycles.

The first wall contact is made at time t_1, the second at t_2, and so on. The return to the initial position x_I takes place between the $2n$th and $(2n+1)$th contacts, which occur at times t_{2n} and t_{2n+1}. Since the orbit is periodic, the $(2n+1)$th contact is at time t_1 after the return to the initial position, so that

$$t_{2n+1} = \frac{2N\pi}{\omega} + t_1. \tag{14}$$

Substituting these conditions into Eq. (3) results in $2n+1$ nonlinear equations for the $2n$ contact times and the initial conditions p_I and x_I that describe a periodic trajectory:

$$\begin{aligned} x_1 &= a_1 + b_1 t_1 + \kappa \cos \omega t_1, \\ -x_1 &= a_2 + b_2 t_2 + \kappa \cos \omega t_2, \\ &\vdots \\ (-1)^{2n+1} x_1 &= a_{2n} + b_{2n} t_{2n} + \kappa \cos \omega t_{2n}, \end{aligned} \tag{15}$$

$$(-1)^{(2n+1)+1} x_1 = a_{2n+1} + b_{2n+1}(2N\pi + t_1) + \kappa \cos \omega t_1. \tag{16}$$

These $2n+1$ equations are nonlinear in the contact times and can only be solved analytically for one initial condition in terms of the other if $n = 1$ or for special cases if $n > 1$. Direct numerical solution for $n > 1$ using current nonlinear solvers also proves impractical or impossible for the large-n nonsymmetric systems that we use to approximate KAM surfaces. We therefore solve the equations numerically with a scheme that iterates on increasingly accurate trial solutions of a linearized form of the equations.

A first choice trial solution at a particular field is found by considering the behavior of the system unperturbed by a driving field. At zero field, all periodic particle trajectories reduce to 1-cycles. Momentum and the time between wall contacts are constant and thus easily determined for an orbit with a rational winding number $\frac{n}{N}$. The momentum at zero field for an (n, N)-cycle is

$$p^0 = \frac{n\omega}{N\pi}. \tag{17}$$

Wall contacts occur at times τ_s given by

$$\tau_s = \frac{[|x_1 - x_I| + 2(s-1)]}{2p^0}. \tag{18}$$

The contact times t_s and initial momentum p_I for a periodic trajectory in a nonzero field can be considered perturbations of the zero-field times and momentum. They are written as

$$\begin{aligned} p_I &= p^0 + \delta_P, \\ t_s &= \tau_s + \delta_s, \qquad s = 1, 2, \ldots, 2n , \end{aligned} \tag{19}$$

where δ_s and δ_P are the perturbations in time and momentum, respectively.

Substituting these expressions for the initial momentum and contact times into the $2n+1$ nonlinear equations of (16) and performing a Taylor expansion to first order in δ_P and δ_s on the resulting system yields a set of $2n+1$ linear equations for the perturbations. They are solved numerically using standard routines from the linear systems package LINPACK [15]. The calculated perturbations are then added to the original trial solution (19) to obtain a new trial solution for the contact times t_i. The new trial solution is substituted into the linearized equations and the process repeated until the solutions converge, that is, until the perturbations become zero within some predetermined precision. This is a variant on Newton's method, similar to those suggested by Mestel and Percival for the standard map and its Hamiltonian equivalents [16] or by Grobgeld *et al.* for the quartic oscillator [17].

We have used this iterative numerical methodology to calculate initial momenta as a function of the field amplitude ϵ for a variety of n and N. The results of these calculations for the initial position at the right-hand wall are shown in Fig. 3. The estimated 1-cycle initial conditions exactly overlay results derived analytically and trajectory calculations of higher-order periodic cycles from initial conditions found by using our iterative scheme replicate the expected periodicity to the precision of the estimation (1.0×10^{-16} in these calculations).

At low energies and high field amplitudes there is some scatter of points in the plot. In those regions or near cycle bifurcations the iterative scheme may converge to a nearby n-cycle characterized by a different time period-

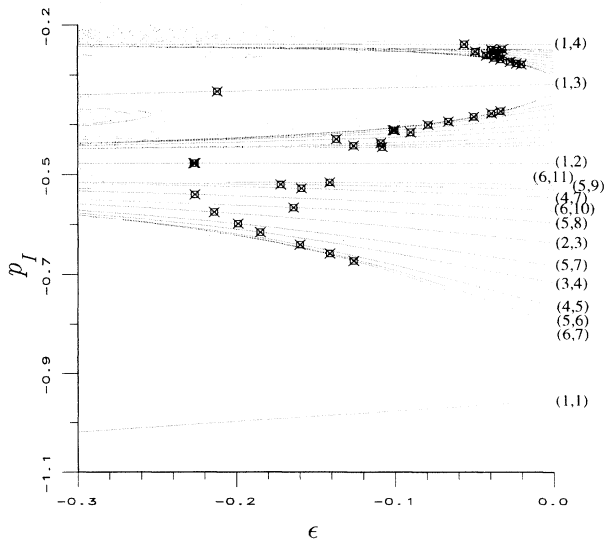

FIG. 3. Initial momentum p_I is plotted as a function of field amplitude ϵ for various (N, n)-cycles. The squares indicate the critical fields at which the cycles become unstable.

icity or a sidebranch of the bifurcation. The scattering occurs for the most part in regions where periodic trajectories are unstable and is therefore of little relevance to the approximation of classical KAM trajectories. However, precision effects may be a cause for concern in extending the approach to the quantum-mechanical system, where "scars" left by unstable periodic orbits are important indicators of the quantum-mechanical states of the system and must thus be calculated accurately. In this case, it may be wise to make a more sophisticated choice of a first trial solution than that suggested here. For example, in a sequence of calculations for an (n, N)-cycle, in which the field is increased in successive increments, a better choice for the starting point at a particular field is the final solution at the previous value.

Figure 3 also illustrates the similarity between regions surrounding the $(1, N)$-cycles. The chief difference is the scale of each $(1, N)$-cycle region. The $(1, N)$-cycles for odd N correspond to the primary resonances of the system, discussed in detail in Sec. V. Cycles and critical fields occur in similar patterns in each resonance zone. This similarity is also apparent in the stroboscopic plots of Fig. 4, where a variety of 4-, 5-, and 6-cycle trajectories is shown. Note that many high-order cycles have low-order equivalents, for example, $(4, 8)$-, $(5, 10)$-, and $(6, 12)$-cycles are all equivalent to the $(2, 1)$-cycle.

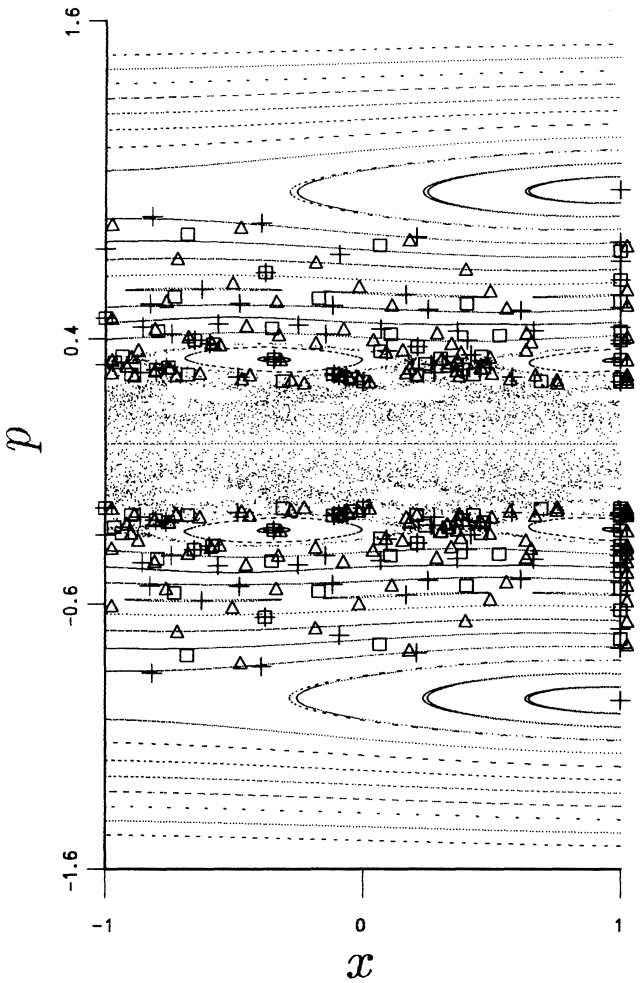

FIG. 4. Stroboscopic plots of various (N, n)-cycles, with momentum p plotted versus position x. Squares mark the center of islands corresponding to 4-cycles, triangles mark the center of islands corresponding to 5-cycles, and crosses mark 6-cycles. Note that for N a multiple of n, the (N, n)-cycles reduce to 1-cycles and similar reductions occur in order when N and n have a common multiple.

IV. STABILITY OF PERIODIC TRAJECTORIES

In a nonlinear Hamiltonian system, a "stable" trajectory is one for which arbitrarily small perturbations do not grow as the motion continues, that is, perturbations remain bounded. Consider the effects of small deviations from the contact times for the $(m + 1)$th full cycle of a periodic trajectory $(m = 0, 1, \ldots)$, where "cycle" in this context refers to a single completed period of the motion rather than the trajectory as a whole. At the beginning of the $(m + 1)$th cycle, the particle will have come in contact with the walls a total of $2mn$ times. The last contact of the mth cycle occurs at

$$t_{2mn} = m\frac{2N\pi}{\omega}. \tag{20}$$

The ith contact of the $(m + 1)$th cycle occurs at

$$t_{2mn+i} = m\frac{2N\pi}{\omega} + t_i. \tag{21}$$

Deviations from the periodic contact times during the $(m + 1)$th cycle can be thought of as some perturbation ξ_{2mn+i} added to the contact time t_{2mn+i}. The perturbed times, denoted by t'_{2mn+i}, are written

$$\begin{aligned}
\omega t'_{2mn+1} &= m(2\pi N) + \xi_{2mn+1} + \omega t_1, \\
\omega t'_{2mn+2} &= m(2\pi N) + \xi_{2mn+2} + \omega t_2, \\
&\vdots \\
\omega t'_{2mn+2n} &= m(2\pi N) + \xi_{2mn+2n} + \omega t_{2n}, \\
\omega t'_{2mn+2n+1} &= (m+1)(2\pi N) + \xi_{2mn+2n+1} + \omega t_1,
\end{aligned} \tag{22}$$

where the equations have been multiplied through by the frequency ω.

Introducing these perturbed times into the three-term recursion relation for the contact times (11) and performing a Taylor expansion on the resulting equations to first order in the deviations ξ_i yields $2n + 1$ linearized equations for ξ_{2nm+i}, written in the form of a three-term recurrence relation as

$$\xi_{2mn+i+2} = A_i\xi_{2mn+i} + B_i\xi_{2mn+i+1} \tag{23}$$

with

$$\begin{aligned}
A_i &= -q_{i,i}/q_{i,i+2}, \\
B_i &= -q_{i,i+1}/q_{i,i+2}.
\end{aligned} \tag{24}$$

The coefficients $q_{i,j}$ are independent of the cycle number m and are given by

$$q_{i,i} = \frac{2x_1(-1)^{i+1} + \kappa(\cos\omega t_{i+1} - \cos\omega t_i)}{[\omega(t_{i+1} - t_i)]^2} + \frac{\kappa \sin\omega t_i}{\omega(t_{i+1} - t_i)}, \tag{25}$$

$$q_{i,i+1} = \frac{-2x_1(-1)^{i+1} + \kappa(\cos\omega t_{i+2} - \cos\omega t_{i+1})}{[\omega(t_{i+2} - t_{i+1})]^2} - \frac{-2x_1(-1)^{i+1} - \kappa(\cos\omega t_{i+1} - \cos\omega t_i)}{[\omega(t_{i+1} - t_i)]^2} + 2\kappa\cos\omega t_{i+1} + \kappa\sin\omega t_{i+1}\left[\frac{1}{\omega(t_{i+2} - t_{i+1})} - \frac{1}{\omega(t_{i+1} - t_i)}\right],$$

$$q_{i,i+2} = \frac{2x_1(-1)^{i+1} - \kappa(\cos\omega t_{i+2} - \cos\omega t_{i+1})}{[\omega(t_{i+2} - t_{i+1})]^2} - \frac{\kappa\sin\omega t_{i+2}}{\omega(t_{i+2} - t_{i+1})}. \tag{26}$$

In general, each solution vector $\vec{\xi} \equiv (\xi_1, \xi_2, \ldots \xi_{2n})$ of a nonperiodic linear three-term recurrence relation of form (23) is associated with two linearly independent solutions $\vec{\zeta}^{(1)}$ and $\vec{\zeta}^{(2)}$ such that the solution $\vec{\xi}$ can be written as a linear combination of the two such that

$$\vec{\xi} = c^{(1)}\vec{\zeta}^{(1)} + c^{(2)}\vec{\zeta}^{(2)}, \tag{27}$$

where $c^{(1)}$ and $c^{(2)}$ are constants [18].

In analogy with Floquet theory for second-order differential equations, we make the ansatz that the components of a solution $\vec{\zeta}$ of the periodic three-term recurrence relation (23) are products of an overall phase factor dependent on the number of cycles the trajectory has completed and a solution Δ_i for the perturbations in a single period,

$$\zeta_{2nm+i} = U_m \Delta_i, \tag{28}$$

where U_m is the characteristic coefficient. The coefficient U_m can be expressed as a product of m phase factors $\mu_1, \mu_2, \ldots, \mu_m$, one for each completed period of an (n, N)-orbit:

$$U_m = \mu_1\mu_2\cdots\mu_m, \tag{29}$$

so that ξ_{2mn+i} becomes

$$\zeta_{2mn+i} = \mu_1\mu_2\cdots\mu_m\Delta_i. \tag{30}$$

A periodic trajectory will remain stable if and only if the perturbations ξ_{2mn+i} are bounded, implying that the linearly independent solutions ζ_{2mn+i} and thus the product of the factors μ_i must also be bounded.

To determine the conditions for which an (n, N)-orbit is stable, Eq. (30) is substituted into the three-term recurrence relation (23). The $(2n+1)$th equation in (22) for t_1 is redundant with the first and the ansatz of Eq. (30) implies that

$$\Delta_{2n+1} = U_m\mu_{m+1}\Delta_1, \quad \Delta_{2n+2} = U_m\mu_{m+1}\Delta_2. \tag{31}$$

These substitutions result in $2n$ fully determined equations for the time deviations in the mth (n, N)-cycle that can be written in matrix form as

$$\vec{\mathbf{0}} = U_m\mathbf{A}\vec{\mathbf{\Delta}}, \tag{32}$$

where the matrix $\mathbf{A}$ is given by

$$\mathbf{A} = \begin{pmatrix} A_1 & B_1 & -1 & 0 & 0 & \cdots & 0 & 0 & 0 & 0 \\ 0 & A_2 & B_2 & -1 & 0 & \cdots & 0 & 0 & 0 & 0 \\ 0 & 0 & A_3 & B_3 & -1 & \cdots & 0 & 0 & 0 & 0 \\ \vdots & \vdots & \vdots & \vdots & \vdots & \vdots & \vdots & \vdots & \vdots & 0 \\ 0 & 0 & 0 & 0 & 0 & \cdots & 0 & A_{2n-2} & B_{2n-2} & -1 \\ -\mu & 0 & 0 & 0 & 0 & \cdots & 0 & 0 & A_{2n-1} & B_{2n-1} \\ \mu B_{2n} & -\mu & 0 & 0 & \cdots & 0 & 0 & 0 & 0 & A_{2n} \end{pmatrix}, \tag{33}$$

and the solution vector $\vec{\mathbf{\Delta}}$ is given by

$$\vec{\mathbf{\Delta}} = \begin{pmatrix} \Delta_1 \\ \Delta_2 \\ \vdots \\ \Delta_{2n-1} \\ \Delta_{2n} \end{pmatrix}. \tag{34}$$

The subscript on the factor μ_{m+1} is dropped, since from Eq. (37) it is clear that μ does not depend on it.

A solution $\vec{\mathbf{\Delta}}$ exists if and only if

$$0 = |\mathbf{A}|. \tag{35}$$

The coefficients $q_{i,j}$ are related by

$$q_{i,i+2} = -q_{i+1,i+1} \tag{36}$$

and, as a consequence, the determinant $|\mathbf{A}|$ can be reduced to a quadratic equation for μ

$$\mu^2 + Q\mu + 1 = 0, \tag{37}$$

where Q is a function of the coefficients A_i, B_i. That is, Q can be expressed in terms of the field amplitude, periodic trajectory contact times, and the initial momentum.

There are two possible solutions of the quadratic equation, given by

$$\mu^{(1,2)} = -\frac{Q}{2} \pm \left(\frac{Q^2}{4} - 1\right)^{1/2}, \tag{38}$$

where the two solutions are related by the expression

$$\mu^{(1)}\mu^{(2)} = 1. \tag{39}$$

Two characterizations for the solutions are possible.

(i) The solutions are complex and each other's conjugates, that is,

$$\mu^{(1)} = [\mu^{(2)}]^* \tag{40}$$

and

$$|\mu^{(1)}| = |\mu^{(2)}| = 1. \tag{41}$$

In this case all solutions ξ_i for the time perturbations (28) are bounded and the trajectory is stable, so that a trajectory whose initial conditions are perturbed slightly from those of the exact periodic trajectory remains on a confined orbit ("island") in the immediate neighborhood of the periodic cycle.

(ii) The μ are real and

$$\mu^{(1)} = (\mu^{(2)})^{-1}\ , \tag{42}$$

so that one or the other of the μ solutions is larger than one. Any solution ξ_i that is not orthogonal to the corresponding Δ_k will increase without bound. Such a periodic trajectory is unstable.

These alternatives are representative of the Hamiltonian nature of the original system. Solutions where both magnitudes of $\mu^{(1,2)}$ are less than one correspond to attractors, which do not exist in Hamiltonian systems.

The parameter Q is real. Therefore, from (37), a periodic trajectory is unstable when

$$\frac{Q^2}{4} - 1 > 0, \tag{43}$$

that is,

$$|Q| > 2, \tag{44}$$

and stable when

$$|Q| < 2. \tag{45}$$

The magnitude of Q thus becomes the criterion by

TABLE I. Critical fields for a variety of (n, N) cycles.

$n=1$	ε_C	$n=2$	ε_C	$n=3$	ε_C	$n=4$	ε_C	$n=5$	ε_C	$n=6$	ε_C
(1,1)	1.2										
										(6,7)	0.128
								(5,6)	0.140		
						(4,5)	0.162				
				(3,4)	0.186						
								(5,7)	0.200		
		(2,3)	0.214								
								(5,8)	0.164		
				(3,5)	0.226						
						(4,7)	0.160				
								(5,9)	0.172		
										(6,11)	0.142
(1,2)	0.228										
										(6,13)	0.108
								(5,11)	0.128		
						(4,9)	0.110				
				(3,7)	0.138						
								(5,12)	0.092		
		(2,5)	0.102								
								(5,13)	0.076		
				(3,8)	0.068						
						(4,11)	0.050				
								(5,14)	0.040		
										(6,17)	0.032
(1,3)	0.212										
										(6,19)	0.020
								(5,16)	0.024		
						(4,13)	0.028				
				(3,10)	0.034						
								(5,17)	0.036		
		(2,7)									
								(5,18)	0.036		
				(3,11)	0.058						
						(4,15)	0.036				
								(5,19)	0.040		
										(6,23)	0.032
(1,4)	0.054										
										(6,25)	0.028
								(5,21)	0.034		
						(4,17)	0.030				
				(3,13)	0.038						
								(5,22)	0.026		
		(2,9)									
								(5,23)	0.024		
				(3,14)	0.021						
						(4,19)	0.016				
								(5,24)	0.013		
										(6,29)	0.008
(1,5)	0.074										

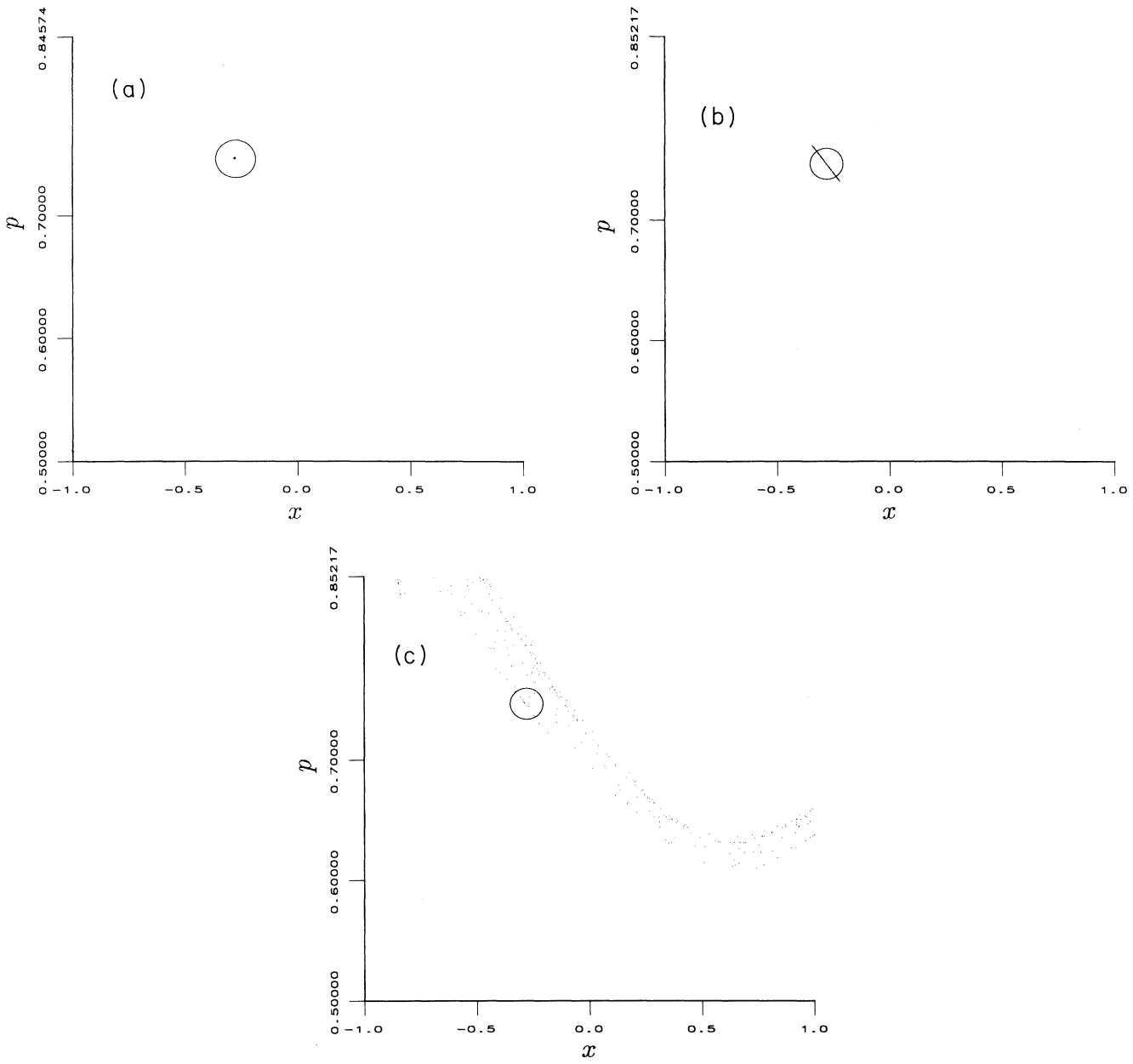

FIG. 5. Stroboscopic plots of the breakup of the $(4,5)$-cycle, predicted to occur at a field amplitude of 0.162. The momentum p is plotted versus the position x. (a) $-\varepsilon = 0.160$, (b) $-\varepsilon = 0.1625$, and (c) $-\varepsilon = 0.165$. The circle indicates the cycle center in all cases.

which we can determine the stability of a periodic trajectory. Given an (n,N)-cycle for which $2n$ contact times and initial momentum have been calculated using the numerical methods described in Sec. III, Q can be calculated numerically from the determinant of the matrix $\mathbf{A}$ (33) and the quadratic equation (37), where the dummy value $|\mu| = 1$ is substituted into the latter. If the resulting value of the parameter $|Q| > 2$, the cycle is unstable at that field; otherwise, it is stable.

We have determined the critical fields at which the trajectories become unstable for a spectrum of (n,N)-cycles by observing when the absolute value of Q becomes greater than 2. The results of these calculations are shown in Table I and Fig. 5. The critical fields determined by this first-order linear stability analysis compare very well to numerical experiments such as that of Fig. 5. A $(4,5)$-cycle trajectory, calculated from initial conditions found by the iterative method, is shown in transition from stable to unstable motion. At less than the critical field, the cycle remains stable after 10 000 wall contacts, appearing as a dot in Fig. 5(a). At a field slightly higher than the critical field amplitude of 0.162, the structure of the invariant tori islands becomes fuzzy and the cycle appears blurred after 3000 steps. Finally,

at well above the critical field, the cycle is entirely unstable and the calculated trajectory merges into the surrounding stochastic layers. Though as a practical matter such numerical experiments are qualitative, our first-order predictions of the onset of instability correspond well to the earliest signs of the disintegration of the islands in the $(4,5)$-cycle.

V. APPROXIMATING KAM SURFACES

We now apply the characterization of the periodic cycles to the problem of approximating KAM tori and predicting their breakdown, using ideas suggested by Escande [9]. Key to this application is Escande's development of the concept of a zoning number that links high-order approximates to the earlier renormalization methodology developed with Doveil to predict KAM breakdown [8]. This original renormalization technique is used by Lin and Reichl [2] to estimate KAM breakdown, but does not allow for representation of the KAM surface itself. The zoning number is analogous in more general systems to the winding number in Hamiltonian equivalents of the standard map [10] and Escande [9] has shown it can be used in similar fashion to determine cyclic approximates to KAM surfaces.

Lin and Reichl [2] write down the Hamiltonian for the cosine-driven particle in an infinite square well as

$$\tilde{H} = \frac{\tilde{p}^2}{2m} + \tilde{b}[\eta(\tilde{x}-a) + \eta(-\tilde{x}-a)] + \tilde{\varepsilon}\tilde{x}\cos\tilde{\omega}(\tilde{t}+\tilde{\phi}) \qquad (b\to\infty)\ , \quad (46)$$

where $\tilde{\varepsilon}$ and $\tilde{\omega}$ are the amplitude and frequency, respectively, of the external field and $\eta(x)$ denotes the unit step function. The constant phase factor $\tilde{\phi}$ is introduced to account for the field phase offset that may exist in a physical system. This Hamiltonian can be transformed into dimensionless form by introducing an arbitrary unit of energy c and the following canonical transformation:

$$\tilde{H} = cH,\quad \tilde{x} = ax,\quad \tilde{p} = \sqrt{2mc}\,p,\quad \tilde{\varepsilon} = \frac{c}{a}\varepsilon,$$
$$\tilde{b} = bc,\quad \tilde{t}+\tilde{\phi} = a\sqrt{\frac{2m}{c}}t,\quad \tilde{\omega} = \frac{1}{a}\sqrt{\frac{c}{2m}}\omega.$$

The resulting Hamiltonian is

$$H = p^2 + b[\eta(x-1) + \eta(-x-1)] + \varepsilon x\cos(\omega t) \qquad (b\to\infty)\ , \quad (47)$$

where the position is normalized to lie on the interval $[-1,1]$ and the transformed momentum p, time t, position x, and all other quantities are now dimensionless.

A canonical transformation to action and angle variables (I,θ), viz.,

$$x = -1 + \frac{2\theta}{\pi}\mathrm{sgn}[\sin(\theta)],\quad p = \frac{\pi I}{2}\mathrm{sgn}[\sin(\theta)]\ , \quad (48)$$

where

$$I = \frac{2\sqrt{E_0}}{\pi},\quad \theta = \frac{\pi^2 I t}{2},\quad \theta\in[-\pi,\pi], \quad (49)$$

and E_0 is the energy and sgn[ ] is the sign of the argument, yields [2]

$$H = \frac{\pi^2 I^2}{4} + \varepsilon x(I,\theta)\cos(\omega t). \quad (50)$$

The position function $x(I,\theta)$ is periodic in I and θ. The Hamiltonian is expanded in terms of a Fourier series

$$H = \frac{\pi^2 I^2}{4} - \frac{4\varepsilon}{\pi^2}\sum_{\substack{n=-\infty\\ n\ \mathrm{odd}}}^{\infty}\frac{1}{n^2}\cos(n\theta-\omega t). \quad (51)$$

In this multiple-resonance form, it is clear that the system has an infinite number of primary resonances at energies E_R

$$\omega = \frac{nd\theta}{dt} = n\pi\sqrt{E_R},\qquad n = 1,3,5,\ldots\ . \quad (52)$$

These are the primary resonances energies, indicated in Fig. 2 by the solid horizontal lines across the phase plane, about which the $(1,N)$-cycles (N odd) are centered.

Primary resonances bound regions of self-similar behavior, that is, the structure of KAM trajectories, stochastic layers, islands, and associated periodic trajectory repeats between primary resonance pairs n and $n+2$. The behavior of a trajectory in this Hamiltonian system is almost completely influenced by the two nearest primary resonances $\hat{n}$ and $\hat{n}+2$ ($\hat{n}$=1,3,...) [2]. It is therefore reasonable to approximate the multiple-resonance Hamiltonian by one of a set of two-resonance Hamiltonians

$$H \approx \frac{\pi^2 I^2}{4} - \frac{4\varepsilon}{\pi^2}\left\{\frac{1}{\hat{n}^2}\cos(\hat{n}\theta-\omega t) + \frac{1}{(\hat{n}+2)^2}\cos[(\hat{n}+2)\theta-\omega t]\right\}. \quad (53)$$

A series of canonical transformations on this two-resonance Hamiltonian leads to the final two-resonance form [2]

$$H' = \frac{v'^2}{2} - \frac{(\hat{n}+2)^2\varepsilon}{2\omega^2}\cos x' - \frac{\hat{n}^2\varepsilon}{2\omega^2}\cos\left[\left(\frac{\hat{n}+2}{\hat{n}}\right)(x'-t')\right]\ , \quad (54)$$

where x', v', and t' are the transformed position, momentum, and time, respectively.

If the parameters M, P, and k are defined as

$$M = \frac{(\hat{n}+2)^2\varepsilon}{2\omega^2},\quad P = \frac{\hat{n}^2\varepsilon}{2\omega^2},\quad k = \frac{\hat{n}+2}{\hat{n}}, \quad (55)$$

this Hamiltonian is clearly of Escande paradigm two-resonance form [9]

$$H' \equiv H_E = \frac{v'^2}{2} - M\cos x - P\cos k(x-t), \quad (56)$$

where M and P are the resonance amplitudes and k is the wave number. Escande [9] defines a stochastic parameter S in terms of the resonance amplitudes M and P by

$$S = 2\sqrt{M} + 2\sqrt{P}. \tag{57}$$

As the parameter is increased, the familiar structure of secondary islands, KAM surfaces, and stochastic layers emerges between the two primary resonances. The winding number describes this hierarchy correctly in the two-resonance special case of the standard map ($M = P = k = 1$), but does not account for the effect of the ratio of spatial periodicities of the two resonances in the more general case. The winding number does not therefore correctly rank trajectories in a general two-resonance system. Escande uniquely characterizes a trajectory's rank in the hierarchy of emerging trajectories by a zoning number z that is the analog of the winding number in systems equivalent to the standard map. This zoning number z is defined as

$$z = k\left(\frac{1}{\bar{v}_P} - 1\right) + 1, \tag{58}$$

where $\bar{v_P}$ is the mean velocity in the paradigm two-resonance system and k is the ratio of primary resonance wave numbers. The zoning number for the paradigm Hamiltonian is rational for periodic cycles and irrational for KAM trajectories.

In two-resonance systems, Escande argues that KAM surfaces whose zoning numbers possess continued fraction expansions ending in the same periodic series of integers form a universal class. The universal class of "noble" tori consists of trajectories possessing zoning numbers with expansions like that of the golden mean $g = (\sqrt{5} + 1)/2$, ending in a series of ones. The golden mean itself is the zoning number of the last KAM between primary resonances to break down. In the special case of the standard map, the zoning number is equal to the inverse winding number, allowing direct comparison of standard map results to the special case of the paradigm two-resonance system.

To relate Escande's work to the multiple-resonance system we reverse the series of transformations leading to the two-resonance paradigm form of the driven square well Hamiltonian (54). We apply this inverse set of transformations to the mean velocity in the paradigm system to obtain an expression for the momentum in the original system in terms of the paradigm velocity v' as

$$\bar{p} = \left[\bar{v}' - \frac{\hat{n}+2}{2}\right]\left[\frac{-2\omega}{(\hat{n}+2)\hat{n}\pi}\right]. \tag{59}$$

The winding number in the original Hamiltonian is given by (12) as

$$\rho = \frac{\bar{v}T}{\lambda} = \frac{\bar{v}2\pi}{4\omega}. \tag{60}$$

Substituting $\bar{v}$ into this expression to relate the winding number ρ to the transformed mean velocity $\bar{v}'$ results in

$$\rho = \frac{2}{\hat{n}}\left[\frac{1}{2} - \frac{\bar{v}'}{\hat{n}+2}\right]. \tag{61}$$

Substitution of the mean velocity as a function of the zoning number (58) into this equation yields the final relation between the winding number of the original system and the zoning number in the final Escande paradigm system:

$$\rho = \frac{1}{\hat{n}}\left[1 - \frac{1}{\hat{n}+2+\hat{n}(z-1)}\right]. \tag{62}$$

Note that the Escande Hamiltonian assumes a mass of 1 and the primed system a mass of $\frac{1}{2}$, accounting for the apparent factor of 2 lost in the transformation from (61) and (62). Because Escande's zoning number depends on the ratio of primary resonance numbers, the zoning number ranks the trajectory not only in the hierarchy of the immediate two resonances, but also in the larger hierarchy of resonances in the multiple resonance system. That is, the zoning or winding number relationship of Eq. (62) is valid for the multiresonance system in its entirety, not just the two-resonance approximation.

We use the final expression (62) relating the driven square well winding number to the Escande two-resonance zoning number to determine the series of periodic trajectory approximations that represent the most robust KAM trajectories in the multiresonance system. The most robust KAM trajectory between primary resonance pairs $\hat{n}$ and $\hat{n}+2$ is characterized by a golden mean zoning number [9]. The winding number of the corresponding KAM surface in the multiresonance system is then given by

$$\rho = \frac{1}{\hat{n}}\left[1 - \frac{1}{\hat{n}+2+\hat{n}(g-1)}\right]. \tag{63}$$

We expand this winding number in successively more accurate continued fraction approximations of the right-hand side of the expression. The result is a series of rational fraction approximates of the winding number. The associated periodic trajectories are the cyclic approximates of the KAM surface itself. Escande notes that for extremely different primary resonance spatial periodicities, a related number such as $g+1$ may be the zoning number of the last KAM trajectory rather than the golden mean itself. The condition on k for which the zoning number of the most robust KAM trajectory is g is given by the rough criterion

$$\frac{1}{k_m} < k < k_m, \tag{64}$$

where

$$k_m \approx 2.2. \tag{65}$$

This condition is always satisfied for the primary resonance pairs in the system of the particle in a square well.

For example, from Eq. (63) the last KAM trajectory between the first and third resonance zones is approximated by periodic cycles with winding numbers

$$\frac{1}{1}, \frac{2}{3}, \frac{3}{4}, \frac{5}{7}, \frac{8}{11}, \frac{13}{18}, \frac{21}{29}, \frac{34}{47}, \cdots . \tag{66}$$

This is the series of cycles, shown in Fig. 6, that was suggested as corresponding to the last KAM trajectory between the first and third resonances by Becker *et al.* [19]. In that work, the series was proposed as a strategic guess based on patterns observed in cyclic trajectories. Similarly, the last KAM trajectory between the third and fifth resonance zones is associated with the series

$$\frac{1}{3}, \frac{4}{15}, \frac{7}{24}, \frac{11}{39}, \frac{18}{63}, \frac{29}{102}, \frac{47}{165}, \cdots, \tag{67}$$

that between the fifth and seventh resonance zones with

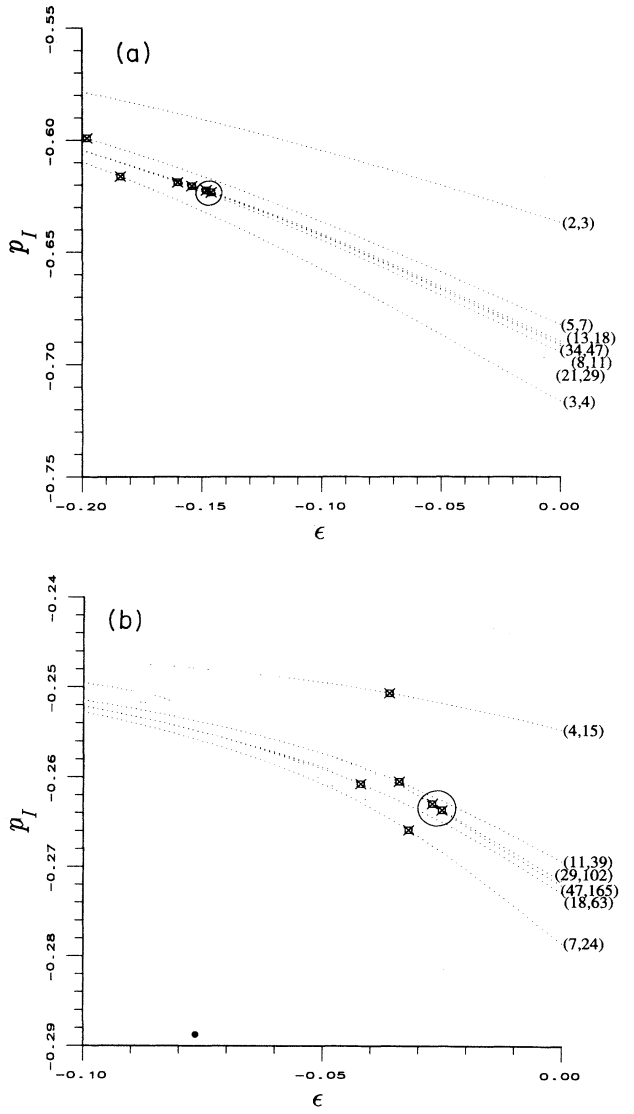

FIG. 6. Initial momenta p_I of cycle approximations to the last KAM surfaces between resonances are plotted as functions of the field amplitude ϵ. In (a), the approximations are for the last KAM surface between resonances one and three; in (b), they are for the approximations to the last KAM surface between resonances three and five. Critical fields are indicated by squares.

TABLE II. Critical fields (ϵ_C) of continued fraction approximations to the last KAM surfaces between resonance zones 1 and 3 and resonance zones 3 and 5 ($\omega = 3$). The predictions for breakdown are $\epsilon_C = 0.143$ and $\epsilon_C = 0.0256$, respectively.

Zones 1–3		Zones 3–5	
ρ	ϵ_C	ρ	ϵ_C
2/3	0.2	4/15	0.037
3/4	0.186	7/24	0.033
5/7	0.196	11/39	0.043
8/11	0.180	18/63	0.043
13/18	0.149	29/102	0.028
21/29	0.155	47/165	0.026
34/47	0.147	76/267	0.027
55/76	0.145	123/432	0.0260
89/123	0.146	199/699	0.0257
144/199	0.144	322/1131	0.0256
233/322	0.143	521/1830	0.0256
377/521	0.144		
610/843	0.143		
987/1364	0.143		

$$\frac{1}{5}, \frac{6}{35}, \frac{11}{60}, \frac{17}{95}, \frac{28}{155}, \frac{45}{250}, \frac{73}{405}, \cdots, \tag{68}$$

and so on.

Finally, we estimate the critical field at which a KAM surface breaks down from the fields at which its periodic approximations become unstable. The estimation increases in accuracy as higher-order approximates are used. We calculate these fields for the most robust KAM trajectories between primary resonance pairs $(1,3)$ and $(3,5)$, estimating the KAM breakdowns from the converging critical cycle fields. The results are summarized in Table II. The breakdown fields compare well to estimates made by direct renormalization (Table III), but are consistently slightly lower. This is probably due to a combination of factors. Lin and Reichl derive their estimates from curves given by Escande and Doveil, directly

TABLE III. Comparison of cyclic-approximation predictions of the critical field to those made using direct renormalization [2] and the overlap criterion [4], as well as to numerical experiments (29 digits of precision [2] and our own 16 digit calculations), $\omega = 3$.

Method	ϵ_C, zones 1–3	ϵ_C, zones 3–5
overlap criterion	0.281	0.0703
renormalization group	0.158	0.0360
cyclic approximations	0.143	0.0256
numerical experiment (29 digits)	0.16–0.17	0.035–0.038
numerical experiment (16 digits)	0.14–0.16	0.025–0.027

for the 1-to-3 transition and by extrapolation for the 3-to-5 transition. Our own use of these curves suggests that such an extrapolation is good to only about 20%. In addition, they quote a higher calculational precision than we use. A higher precision calculation takes many more iterations to exhibit diffusion across the energy spectrum, so that breakdown at a given number of iterations appears to occur at a higher field for greater precision. For all practical purposes, however, critical fields to more than two or three digits of precision are probably not verifiable by numerical experiment. The virtue of our current approach lies less in the more precise prediction of the breakdown fields than in the ability to approximate the KAM surface itself.

VI. CONCLUSIONS

We have presented a complete characterization of the periodic trajectories of the driven square well and established criteria by which their stability can be determined. Our first-order estimate of those critical fields compares closely to those found by numerical experiment. The difficulty in performing a similar analysis of the KAM surfaces of the system is that they are associated with irrational winding numbers and therefore cannot be treated directly using numerical methods of the type we use to describe periodic cycles. However, using Escande's ideas for approximating KAM surfaces in the two-resonance system and our description of the periodic

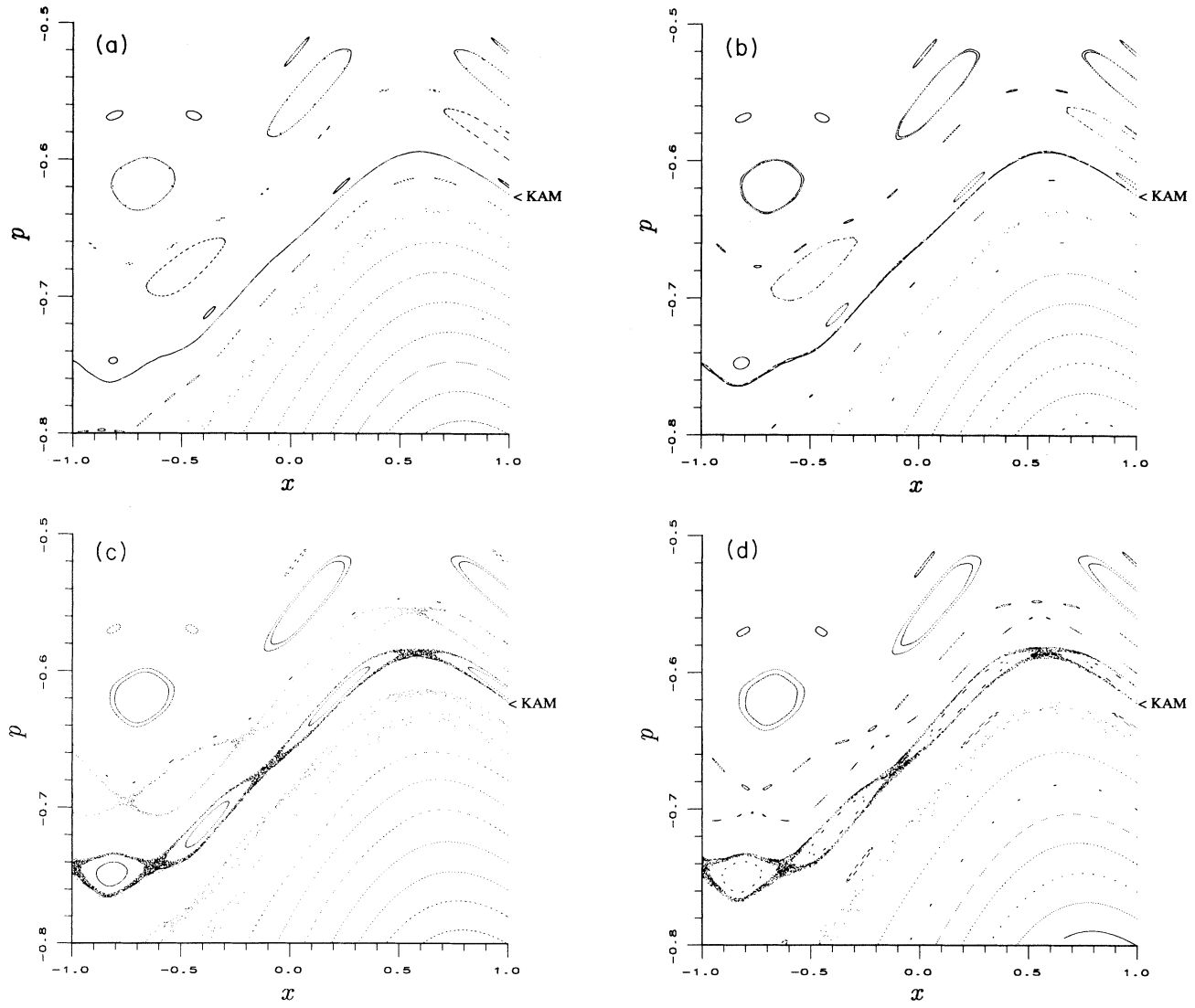

FIG. 7. These stroboscopic phase plane plots show the breakdown of the last KAM surface between the first and third resonances and the accompanying transition to global instability. Momentum p for the trajectories is plotted versus position x. The field amplitude is (a) 0.142, (b) 0.144, (c) 0.148, and (d) 0.150. The critical field is estimated to be 0.143. The nearly solid line of trajectory approximations in (a) and (b) indicates the position before breakdown of the last KAM surface between the resonances (Fig. 6). All trajectories are calculated from an initial position $x_I = 1$ for 2000 time steps.

trajectories of the driven square well, we have been able to model the most robust KAM surfaces, those associated with the transition from local to global stochasticity (Fig. 7). We have made accurate estimates of the breakdowns of these "last" KAM surfaces from the critical fields at which their high-order cyclic approximations become unstable. These breakdown estimates generally improve upon those made using overlap criteria or direct renormalization techniques. However, the principal advantage of this approach is the ability to represent the KAM surface itself in terms of cyclic approximates, information that could not be derived directly using other methods. This capability, together with the analysis of the periodic trajectories themselves, gives us a highly detailed description of the classical system.

The utility of this description is not limited to increasing our understanding of a single classical Hamiltonian system. The approach discussed here should be applicable to other multiple-resonance systems. More significantly, Lin and Reichl extended their original work on the classical system in a study of resonance overlap in the quantum regime [11,12], but to our knowledge the periodic trajectories have not yet been related to the localization of quantum wave functions in the driven square well. Theoretical studies [7,20] have shown that periodic orbits of nonlinear systems are an extremely useful tool for creating descriptions of their semiclassical and quantum dynamics. Analyses of semiclassical spectra can be performed in terms of stable and unstable periodic cycles and it has been shown in quantum-mechanical calculations that wave functions often appear to be localized in the region of unstable periodic orbits ("scars") in chaotic systems. We have recently applied these ideas, together with the description of classical periodic trajectories and KAM surfaces presented in this paper, to the quantum system. In work described in a future paper, we discuss this application to the determination of possible candidates for a quantum resonance that is the quantum equivalent of the classical KAM surface.

[1] W. Becker and J.K. McIver, Phys. Lett. **121**, 286 (1987).
[2] W.A. Lin and L.E. Reichl, Physica D **19**, 145 (1986).
[3] L.E. Reichl, *The Transition to Chaos In Conservative Classical Systems: Quantum Manifestations* (Springer-Verlag, New York, 1992).
[4] B. Chirikov, Phys. Rep. **52**, 263 (1979).
[5] A.J. Lichtenberg and M.A. Lieberman, *Regular and Stochastic Motion* (Springer-Verlag, New York, 1983).
[6] Alfredo M. Orzorio de Almeida, *Hamiltonian Systems: Chaos and Quantization* (Cambridge University Press, Cambridge, 1988)
[7] M.C. Gutzwiller, *Chaos in Classical and Quantum Mechanics* (Springer-Verlag, Berlin, 1990).
[8] D.F. Escande and F. Doveil, J. Stat. Phys. **26**, 257 (1981).
[9] D.F. Escande, Phys. Rep. **121**, 165 (1985).
[10] J.M. Greene, J. Math. Phys. **20**, 1183 (1979).
[11] L.E. Reichl and W.A. Lin, Phys. Rev. A **33**, 3598 (1986).
[12] W.A. Lin and L.E. Reichl, Phys. Rev. A **37**, 3972 (1988).
[13] M.Z. Fuka and J.K. McIver (unpublished).
[14] M.Z. Fuka, Ph.D. dissertation, University of New Mexico, 1994.
[15] J.J. Dongarra *et al.*, LINPACK User's Guide, Philadelphia Society for Industrial and Applied Mathematics, 1979.
[16] Ben Mestel and Ian Percival, Physica D **24**, 172 (1987).
[17] Dov Grobgeld, Eli Pollak, and Jakub Zakrzewski, Physica D **56**, 368 (1992).
[18] W.B. Jones and W.J. Thron, *Continued Fractions: Analytical Theory and Applications* (Addison-Wesley, Reading, MA, 1980).
[19] W. Becker, M. Fuka, J.K. McIver, M. Orszag, and R. Ramirez, *Instabilities and Nonequilibrium Structures III*, (Kluwer Academic, Dordrecht, 1991), pp. 43–57.
[20] Rainer Scharf and Bala Sundaram, Phys. Rev. A **46**, 3164 (1992).